

Intrachain collinear magnetism and interchain magnetic phases in Cr_3As_3 -K-based materials

Giuseppe Cuono ^{1,*}, Filomena Forte,^{2,3} Alfonso Romano ^{3,2}, Xing Ming ⁴, Jianlin Luo,^{5,6,7}
Carmine Autieri ^{1,2,†} and Canio Noce ^{5,2}

¹International Research Centre Magtop, Institute of Physics,

Polish Academy of Sciences, Aleja Lotników 32/46, PL-02668 Warsaw, Poland

²Consiglio Nazionale delle Ricerche CNR-SPIN, Università degli Studi di Salerno, I-84084 Fisciano (Salerno), Italy

³Dipartimento di Fisica “Eduardo Renato Caianiello,” Università degli Studi di Salerno, I-84084 Fisciano (Salerno), Italy

⁴College of Science, Guilin University of Technology, Guilin 541004, China

⁵Beijing National Laboratory for Condensed Matter Physics and Institute of Physics,
Chinese Academy of Sciences, Beijing 100190, China

⁶Songshan Lake Materials Laboratory, Dongguan, Guangdong 523808, China

⁷School of Physical Sciences, University of Chinese Academy of Sciences, Beijing 100190, China



(Received 11 August 2020; revised 22 April 2021; accepted 5 May 2021; published 2 June 2021)

We perform a comparative study of the KCr_3As_3 and the $\text{K}_2\text{Cr}_3\text{As}_3$ quasi-one-dimensional compounds and show that the strong interplay between the lattice and the spin degrees of freedom promotes a collinear ferromagnetic ground state within the chains in the presence of intrachain antiferromagnetic couplings. We propose that the interchain antiferromagnetic coupling in KCr_3As_3 plays a crucial role in the experimentally observed spin-glass phase with low critical temperature. In the same region of the parameter space, we predict $\text{K}_2\text{Cr}_3\text{As}_3$ to be nonmagnetic but on the verge of magnetism, sustaining interchain ferromagnetic spin fluctuations while the intrachain spin fluctuations are antiferromagnetic.

DOI: [10.1103/PhysRevB.103.214406](https://doi.org/10.1103/PhysRevB.103.214406)

I. INTRODUCTION

Recently, bulk superconductivity in $\text{K}_2\text{Cr}_3\text{As}_3$ with $T_c = 6.1$ K has been reported, this representing the first observation of superconductivity in Cr-based compounds at ambient pressure [1]. Following this discovery, three additional superconductors in the series $A_2\text{Cr}_3\text{As}_3$, with $A = \text{Na}$ [2], Rb [3], and Cs [4], have been synthesized, with superconducting critical temperatures equal to 8.6, 4.8, and 2.2 K, respectively. This is a new family of superconductors, likely to be unconventional [5–11], which, differently from the previously discovered Cr-based superconductor CrAs [12–21], exhibits a quasi-one-dimensional crystal structure, with infinite $[(\text{Cr}_3\text{As}_3)^{2-}]_\infty$ linear chains of double-walled subnanotubes (DWSNs), interconnected by A^+ cations [1–4]. In particular, the role played in these compounds by the reduced dimensionality in conjunction with the electronic correlations is currently the subject of intense investigation [22–28]. We also point out interesting analogies between the properties of the above-mentioned one-dimensional Cr-based superconductors and the family of MQ_2 ($M = \text{Nb}, \text{Ta}$; $Q = \text{S}, \text{Se}$) superconductors with one-dimensional spectrum [29] and star-of-David clusters [30–32].

Almost at the same time, a parent compound series has been synthesized, namely, $A\text{Cr}_3\text{As}_3$ ($A = \text{K}, \text{Rb}, \text{Cs}$), which, according to some authors, does not exhibit superconductiv-

ity but a spin-glass-like magnetism [33], while according to other authors it presents bulk superconductivity [34,35]. It is argued that superconductivity arises both in KCr_3As_3 [34] and RbCr_3As_3 [35] upon post-treatment with a hydrothermal annealing in pure dehydrated ethanol, this leading to an improvement in the sample crystallinity. Recently, Taddei *et al.* [36] detected a previously missed effect of the ethanol bath alkaline ion deintercalation. They suggest that the difference between nonsuperconducting spin-glass and nonmagnetic superconducting samples is not related to the sample crystallinity but rather to the amount of intercalated hydrogen [36,37]. In this context, a more effective way of intercalating hydrogen in KCr_3As_3 has very recently been realized via electrochemical hydrogenization in KOH solution at about 75°C . This procedure led to the fabrication of samples which exhibit a novel phase separation regime where a minority superconducting phase with T_c as high as 5.8 K coexists with a majority nonsuperconducting one [38].

Therefore both the $A_2\text{Cr}_3\text{As}_3$ and the $A\text{Cr}_3\text{As}_3$ families still need a deep analysis to better understand the interplay between structural, magnetic, and superconducting properties.

As far as magnetism is concerned, in the case of $\text{K}_2\text{Cr}_3\text{As}_3$, first-principles calculations [39] suggest that the triangular geometry tends to frustrate antiferromagnetism, so that the nonmagnetic phase is the most stable one. On the other hand, Wu *et al.* [40] predict that $\text{K}_2\text{Cr}_3\text{As}_3$ and $\text{Rb}_2\text{Cr}_3\text{As}_3$ possess strong frustrated magnetic fluctuations and are near a novel in-out coplanar magnetic ground state. Interestingly, magnetism increases in the $A_2\text{Cr}_3\text{As}_3$ compounds when we go from the K to the heavier Cs. Nuclear quadrupole resonance

*gcuono@magtop.ifpan.edu.pl

†autieri@magtop.ifpan.edu.pl

measurements on the $A_2\text{Cr}_3\text{As}_3$ family indicate that going along the series $A = \text{Na}, \text{Na}_{0.75}\text{K}_{0.25}, \text{K}, \text{Rb}$, the system tends to approach a possible ferromagnetic quantum critical point [41]. For KCr_3As_3 , Bao *et al.* [33] report that the effective magnetic moment is $0.68 \mu_B/\text{Cr}$, with a susceptibility that below 56 K exhibits a behavior deviating from the standard Curie-Weiss one. In the same temperature range a rapid increase in the resistivity is also found, this suggesting the formation of spin clusters. Moments then freeze into a spin-glass state below $T_f = 5$ K, as also signaled by the behavior of the specific heat, which, as in other spin-glass systems, shows a peak slightly above T_f [33]. These results seem to be related to the geometrical frustration between the Cr local spins, though the microscopic origin of the spin-glass phase is not addressed.

Very recently, neutron total scattering and density functional theory (DFT) studies [42] have revealed significant phonon instabilities, associated with a frustrated orthorhombic distortion in $\text{K}_2\text{Cr}_3\text{As}_3$. Large atomic displacement parameters with anomalous temperature dependencies have been found, which result from highly localized orthorhombic distortions of the CrAs sublattice and coupled K displacements [42]. The Cr triangles in the double-walled subnanotubes are no longer equilateral, which could lead to the release of magnetic frustration. These results suggest a more complex phase diagram with a subtle interplay of structural, electron-phonon, and magnetic interactions. Further investigation is thus needed for $\text{K}_2\text{Cr}_3\text{As}_3$ as well as for other superconductors belonging to the same class, with the aim of understanding to what extent their superconducting behavior should be considered unconventional. A lattice instability has also been found in KCr_3As_3 , corresponding to a distortion of the Cr metallic wires in the crystal structure. This distortion couples strongly to both the electronic and the magnetic properties [43,44].

In this paper we address how the magnetic properties of $\text{K}_2\text{Cr}_3\text{As}_3$ and KCr_3As_3 change by taking into account the distortions predicted in recent literature [42]. We investigate the magnetism in both compounds, in the case where deformations of the chromium ion triangles consistent with the orthorhombic distortions are considered.

We use a DFT approach, also including the Coulomb repulsion U , to explore the most favorable magnetic configurations inside the chains and between the chains. We get the optimized crystal structure and show that the strong interplay between the lattice and the spin degrees of freedom promotes a collinear ferrimagnetic ground state within the chains. We propose that the experimentally observed spin-glass phase at low temperature in KCr_3As_3 can be attributed to geometric frustration of antiferromagnetic coupling among the chains. Moreover, we show that the $\text{K}_2\text{Cr}_3\text{As}_3$ nonmagnetic state is in close proximity to a ferrimagnetic phase, due to the ferromagnetic interchain magnetic exchange emerging in a regime of moderate electronic correlations.

The paper is organized as follows: In Sec. II we describe in detail the crystal structures of $\text{K}_2\text{Cr}_3\text{As}_3$ and KCr_3As_3 , in Sec. III we report the computational details of our approach, Sec. IV is devoted to the magnetic properties inside the subnanotubes, in Sec. V we introduce a Heisenberg model for the magnetic exchanges inside the chain, in Sec. VI we present

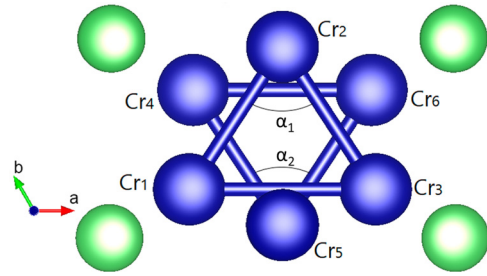


FIG. 1. Cr triangles belonging to the $[(\text{Cr}_3\text{As}_3)^{2-}]_\infty$ subnanotubes, in the distorted case. Blue and green spheres denote Cr and As atoms, respectively.

a comparative analysis between $\text{K}_2\text{Cr}_3\text{As}_3$ and KCr_3As_3 , showing the results emerging when the magnetic interactions between the chains are considered, and finally, Sec. VII is devoted to a summary discussion and to the conclusions.

II. CRYSTAL STRUCTURE OF Cr_3As_3 -CHAIN-BASED K MATERIALS

The crystal structure of $\text{K}_2\text{Cr}_3\text{As}_3$ is quasi-one-dimensional, according to the needlelike morphology experimentally verified using single-crystal x-ray diffraction [1]. The structure contains infinite $[(\text{Cr}_3\text{As}_3)^{2-}]_\infty$ linear chains of DWSNs, interconnected by K^+ cations (see Fig. 1). Cr atoms should bond covalently with As, whereas As should bond ionically with K^+ , separating electropositive Cr and K atoms. The $[(\text{Cr}_3\text{As}_3)^{2-}]_\infty$ DWSNs are composed of inner Cr_3 twisted tubes and outer As_3 ones, which are constructed by the face-sharing Cr_6 (or As_6) octahedra along the crystallographic c direction [1]. Since the Cr sublattices may carry magnetic moments, one expects strong geometric magnetic frustration.

The $[(\text{Cr}_3\text{As}_3)^{2-}]_\infty$ DWSNs and the K^+ cations form a hexagonal lattice with the space group $P\bar{6}m2$. Every unit cell contains 2 f.u., the chemical formula of one unit cell being $\text{K}_4\text{Cr}_6\text{As}_6$. We note that all the atoms occupy the crystalline planes $z = 0$ and $z = 0.5$, with the two crystallographically different K sites, namely, K_1 and K_2 , located at $z = 0.5$ and $z = 0$, respectively. This arrangement leads to the absence of inversion symmetry as well as to the loss of sixfold rotation symmetry. Correspondingly, there exist two inequivalent As and Cr sites.

The $\text{K}_2\text{Cr}_3\text{As}_3$ material is not stable since chemically it deteriorates easily at ambient conditions. However, by means of a topotactic reaction, which keeps the Cr_3As_3 chains unmodified, one gets the corresponding parent compound KCr_3As_3 , which, in contrast, is stable in air. This compound loses two K ions in a unit cell, and correspondingly, the lattice parameters a and c of KCr_3As_3 decrease by 9 and 1%, respectively, compared with those of $\text{K}_2\text{Cr}_3\text{As}_3$. More importantly, there is only one site for K ions, which changes the point group from D_{3h} to C_{6h} and the space group from $P\bar{6}m2$ (No. 187) [1] to $P6_3/m$ (No. 176) [33]. Owing to the symmetry, all the Cr triangles in the ab plane have exactly the same size. Thus we may guess that the different space group could affect in a distinct way the electronic and magnetic properties of the two different K-based materials.

III. APPROACH AND COMPUTATIONAL DETAILS

We have performed DFT calculations by using the Vienna *ab initio* simulation package (VASP) [45–47]. The core and the valence electrons were treated within the projector augmented wave (PAW) [48] method with a cutoff of 440 eV for the plane-wave basis. For calculations concerning the interactions inside a single chain, we have used the PBEsol exchange-correlation method [49], a revised Perdew-Burke-Ernzerhof (PBE) generalized gradient approximation (GGA) that improves equilibrium properties of solids. This choice is motivated by the fact that the functional used within PBEsol is the most suited for the relaxation and in this system the relaxation is fundamental. These calculations have been performed using a $4 \times 4 \times 10k$ -point grid, in such a way as to have 160 k points in the first Brillouin zone.

In DFT, electronic interaction energies are simply described as the sum of the classical Coulomb repulsion between electronic densities in a mean-field approximation, via the Hartree term, and the exchange-correlation term that is supposed to encompass all the correlations and spin interactions. This approach has proved to be quite efficient in studies of weakly correlated materials. When moderately and strongly correlated electron systems are instead considered, an additional Coulomb repulsion U is added to the energy functional [50]. The local-density approximation + U (LDA + U) increases the magnetic moment with respect to the LDA. In metallic systems, large values of U may give rise to an overestimation of the magnetic moment, so that, in the case of moderate correlations, quite small values of the Coulomb repulsion are usually required to reproduce the experimental results. We also remind the reader that in metallic compounds the Fermi screening is expected to reduce the electrostatic repulsion.

PBEsol + U is actually the approach that we have followed here to take into account the correlations associated with the Cr 3d states. The DFT + U method can give unrealistic magnetic orders for large U . However, to avoid this, the values of U specifically suited for the investigation of $\text{K}_2\text{Cr}_3\text{As}_3$ and KCr_3As_3 have been selected on the basis of a scanning of the magnetic moment as a function of the Coulomb repulsion. Starting from the fact that for $U = 0$ we always get a vanishing magnetic moment, we consider gradually increasing values of U , in this way reproducing the entire spectrum of the magnetic moment values. Comparing the obtained results with the experiments, we came to the conclusion that within our theoretical setup a suitable value of the effective Coulomb repulsion is $U = 0.3$ eV for both compounds. Regarding the Hund coupling, which as is well known plays a relevant role in many metallic systems [51], we have used the value $J_H = 0.15U$, in agreement with approaches based on the constrained random phase approximation for d electrons [52].

In the numerical procedure we have relaxed the lattice constants and the internal atomic positions, with the forces that have been minimized to less than 0.01 eV/Å in the structural relaxation. To avoid adding an additional degree of freedom, we have fixed the volume of the unit cell to its experimental value and then performed the relaxation of the atomic positions. For the calculations between different chains, we have used the PBEsol, the LDA, and the strongly constrained and

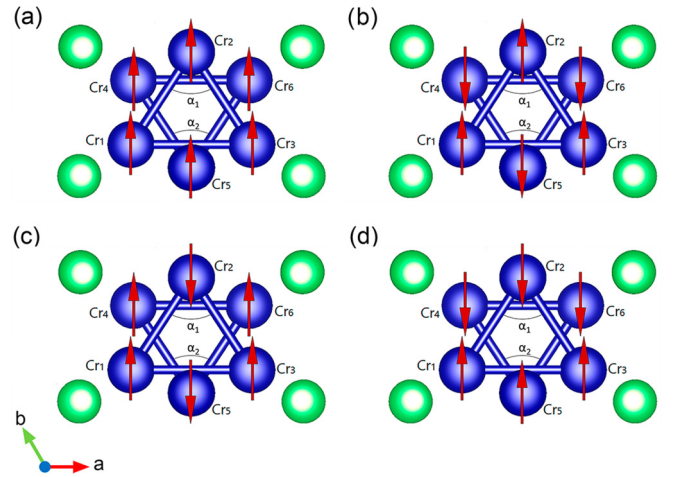


FIG. 2. Cr spin configurations investigated in this paper. We have defined these states as (a) the ferromagnetic state (FM), (b) the interlayer antiferromagnetic state (AFM), (c) the up-up-down/up-up-down ($\uparrow\uparrow\downarrow\uparrow\uparrow\downarrow$) stripe state, and (d) the up-up-down/down-down-up ($\uparrow\uparrow\downarrow\downarrow\downarrow\uparrow$) zigzag state.

appropriately normed meta-GGA (SCAN meta-GGA) [53]. These calculations have been performed using a $2 \times 4 \times 10k$ -point grid and thus 80 k points in the first Brillouin zone; we have halved the number of k points along the x direction because the number of cells along x has doubled. The values of the lattice constants of $\text{K}_2\text{Cr}_3\text{As}_3$ are $a = 9.9832$ Å and $c = 4.2304$ Å [1], and those of KCr_3As_3 are $a = 9.0909$ Å and $c = 4.1806$ Å [33].

IV. *Ab initio* MAGNETIC PROPERTIES OF $[(\text{Cr}_3\text{As}_3)^{2-}]_\infty$ SUBNANOTUBES

It is well established that the significant phonon instability found in $\text{K}_2\text{Cr}_3\text{As}_3$ may give rise to a frustrated orthorhombic distortion [42]. This implies that the Cr triangles in the DWSNs are no longer equilateral, likely leading to a subtle interplay between the magnetic frustration and the structural properties of the material.

To investigate this issue, we have performed the atomic relaxation of the distorted triangles composed of Cr atoms and belonging to the $[(\text{Cr}_3\text{As}_3)^{2-}]_\infty$ subnanotubes, for different values of the Coulomb repulsion U . The relaxation procedure has been done starting from both collinear and non-collinear magnetic configurations. In the undistorted phase, assuming an initial noncollinear magnetic configuration, convergence is reached maintaining this kind of configuration. Performing the same procedure in the distorted phase, the system converges instead to a collinear magnetic configuration, thus implying that in this case the noncollinear solution is metastable. Therefore the attainable magnetic configurations here considered are planar-collinear arrangements of the Cr magnetic moments within the unit cell in the DWSNs. Our DFT analysis shows that in the presence of U these collinear phases are the magnetic stable states, instead of the noncollinear ones previously predicted [39,40]. They are reported in Fig. 2 and correspond to the ferromagnetic state (FM), the interlayer antiferromagnetic state (AFM), the

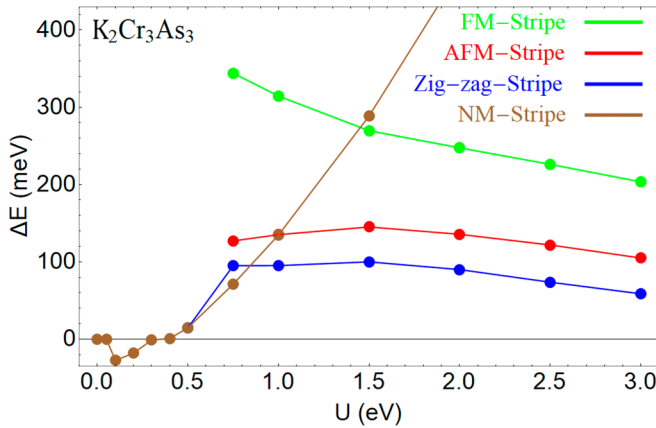


FIG. 3. Energy per Cr atom of the FM, AFM, zigzag, and NM states measured with respect to the stripe state as a function of the Coulomb interaction for the $\text{K}_2\text{Cr}_3\text{As}_3$ compound. At low values of U , data for the FM and the AFM phases are not shown due to the lack of convergence of the numerical procedure in that regime.

up-up-down/up-up-down stripe state ($\uparrow\uparrow\downarrow\text{-}\uparrow\uparrow\downarrow$), and the up-up-down/down-down-up zigzag state ($\uparrow\uparrow\downarrow\text{-}\downarrow\downarrow\uparrow$). Together with these, we also consider the nonmagnetic (NM) state. We point out that the notation adopted for the atoms and the angles of the Cr triangles is the same as that reported in Fig. 1. Thus the configurations considered in our calculations are represented in Fig. 2. In this figure, Cr_1 , Cr_2 , and Cr_3 indicate the Cr atoms belonging to the $z = 0$ plane, whereas Cr_4 , Cr_5 , and Cr_6 are the Cr atoms in the $z = 0.5$ plane. Moreover, the angle α_1 (α_2) is the angle at the vertex of the triangle of the plane $z = 0$ ($z = 0.5$). In the distorted case the Cr atoms at different planes are closer than in the undistorted case, so that, for instance, the $\text{Cr}_2\text{-Cr}_4$ and the $\text{Cr}_2\text{-Cr}_6$ distances become shorter. Therefore the coupling between the atoms at $z = 0$ and $z = 0.5$ is stronger, affecting in a different way the electronic properties as well as the magnetic couplings, as shown in Appendixes A and B. In Secs. IV A and IV B we will present our numerical DFT calculations for the two $[(\text{Cr}_3\text{As}_3)^{2-}]_\infty$ DWSNs in $\text{K}_2\text{Cr}_3\text{As}_3$ and KCr_3As_3 , respectively.

A. $\text{K}_2\text{Cr}_3\text{As}_3$

In Fig. 3 we plot the energy of the above-mentioned configurations as a function of the Coulomb repulsion U , evaluated with respect to the energy of the stripe state. We observe that for values of the Coulomb repulsion $U < U_c = 0.4$ eV, the ground state is nonmagnetic, then becoming the stripe one for $U \geq U_c$. We also note that the energy of the ferromagnetic configuration is always larger than the other collinear considered phases.

Figures 4 and 5 report the behavior as a function of U of the angles α_1 and α_2 shown in Fig. 2 and of the four inequivalent magnetic moments of the Cr ions, respectively. From these figures, we deduce that the system is characterized by a strong interplay between lattice and spin degrees of freedom, implying that it is not possible to decouple the magnetic properties from the structural ones. Indeed, we can see from Fig. 4 that, apart from the FM configuration, the other possible magnetic

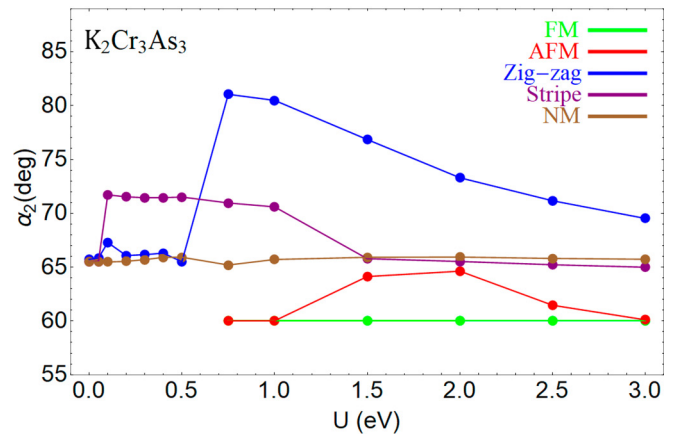
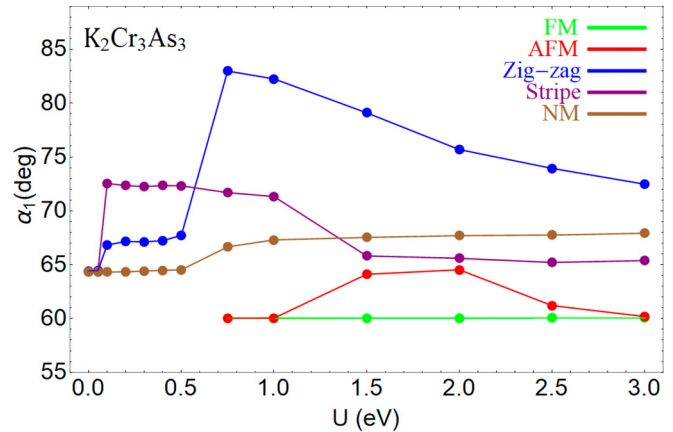


FIG. 4. Angles of the Cr triangles in $\text{K}_2\text{Cr}_3\text{As}_3$ as functions of the Coulomb interaction. In the upper panel, α_1 is the angle at the vertex of the Cr triangle located at $z = 0$, while in the lower panel, α_2 is the same angle for the triangle located at $z = 0.5$.

states always correspond to distorted triangles, with a distortion which for U larger than 0.5 eV is particularly pronounced in the zigzag phase. We also note that above $U = 1.5$ eV there are no more structural effects on the stripe phase, whereas for the other magnetic configurations there is still a dependence of α_1 and α_2 on the Coulomb repulsion. Importantly, this trend is quite similar for the triangles located at $z = 0$ and $z = 0.5$. When lower values of U are considered, we observe that the lowest-energy NM and stripe phases correspond to distorted triangles, with the angles α_1 and α_2 staying unaffected upon variations in the Coulomb repulsion U .

As far as the magnetic moments of the four inequivalent Cr sites are concerned, we may distinguish, as for the angle variations, a different behavior in the two regimes corresponding to values of U approximately lower and higher than 1.5 eV, respectively (see Fig. 5). For $U \gtrsim 1.5$ eV the magnetic moment at any Cr site is quite large, assuming a value around $3 \mu_B$ regardless of the magnetic configuration under consideration. We also note that with increasing U these magnetic moments approach the maximum predicted value for Cr ions in the $\text{K}_2\text{Cr}_3\text{As}_3$ compound, which is $3.33 \mu_B$. Indeed, since we have K^{+1} and As^0 with empty Cr $4s$ levels, the valence of the chromium is 6.67 while the oxidation state is $+2/3$ in $\text{K}_2\text{Cr}_3\text{As}_3$. On the other hand, at low values of U the Cr-ion

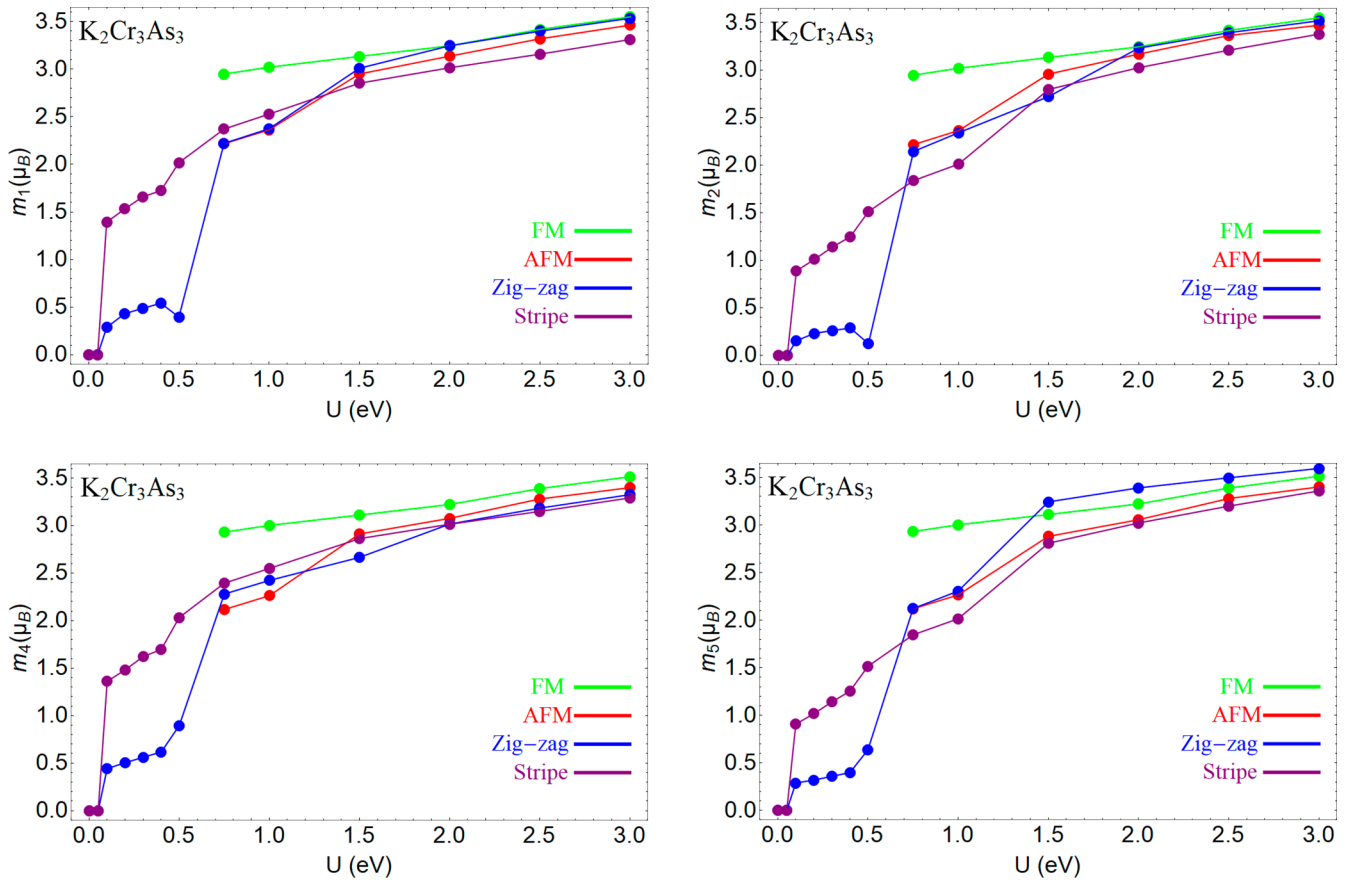


FIG. 5. Magnetic moments of the Cr ions for the configurations shown in Fig. 2, as functions of the Coulomb interaction for the $\text{K}_2\text{Cr}_3\text{As}_3$ compound.

magnetic moments tend to vanish in the zigzag as well as in the stripe phase, thus providing evidence of a nonmagnetic ground-state configuration.

B. KCr_3As_3

Let us now discuss the results obtained for KCr_3As_3 . We will refer here to the same notation used in Sec. IV A.

We have plotted in Fig. 6 the energies of the various phases as functions of U , evaluated as in Fig. 3 with respect to the energy of the stripe-phase state. We find that the NM state is the ground state for $U \lesssim U_c = 0.3$ eV, whereas for $U \gtrsim U_c$ the ground state is the stripe-phase state, as in the case of $\text{K}_2\text{Cr}_3\text{As}_3$.

Differently from $\text{K}_2\text{Cr}_3\text{As}_3$, where we have one layer of K_1 and one of K_3 , in KCr_3As_3 the two layers at $z = 0$ and $z = 0.5$ are equivalent, and so are the vertex angles and the corresponding Cr atoms belonging to the adjacent planes. We plot in Fig. 7 the value of the vertex angle of the triangle located at $z = 0$. In the stripe configuration this angle does not vary significantly with increasing U , implying a quite robust stable configuration against variations in the Coulomb repulsion. Looking at the local magnetic moments (Fig. 8), we find, as in $\text{K}_2\text{Cr}_3\text{As}_3$, two distinct behaviors in the regimes of low and high values of U . Indeed, for $U \lesssim 0.5$ eV the zigzag and the AFM phases exhibit a vanishing local magnetic moment, whereas in the stripe configuration a finite value is found also

at $U = 0$. On the other hand, for large U the magnetic moments approach the maximum value predicted for chromium ions in the KCr_3As_3 compound, which is $3.67 \mu_B$, due to a valence of 6.33 electrons and a corresponding oxidation state equal to $+1/3$.

Since it has been experimentally found that KCr_3As_3 has a finite magnetic moment, approximately equal to $0.68 \mu_B$ [33],

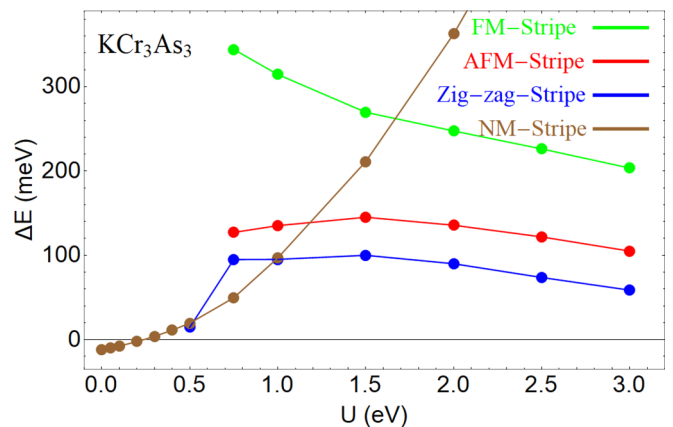


FIG. 6. Energy per Cr atom of the FM, AFM, zigzag, and NM states measured with respect to the stripe state, as a function of the Coulomb interaction for the KCr_3As_3 compound.

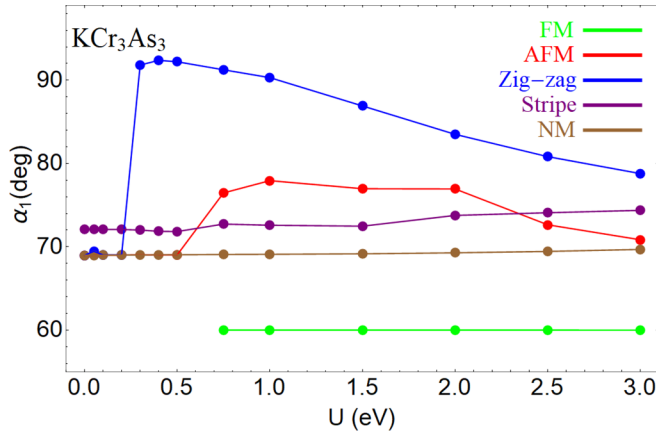


FIG. 7. Angle at the vertex of the Cr-atom triangle at $z = 0$ as a function of the Coulomb interaction for the KCr_3As_3 compound.

we can say that our results are consistent with a picture of KCr_3As_3 being in a moderately correlated ground state of the stripe type where U is approximately equal to 0.3 eV and the predicted value of the magnetic moment is finite, though slightly larger ($\sim 1.1 \mu_B$) than the above-mentioned experimental one. In addition, the degree of distortion of the triangles forming the DWSNs is in this state predicted to be 72° , as one can see from Fig. 7.

V. HEISENBERG MODEL FOR MAGNETIC EXCHANGES INSIDE THE CHAIN

The DFT analysis described above demonstrated that the lowest-energy magnetic configurations within the DWSNs are stable already for low values of the on-site Coulomb repulsion. Also, the magnetic susceptibility measurements suggest dominantly antiferromagnetic interactions between local moments at Cr sites at least in $\text{K}_2\text{Cr}_3\text{As}_3$ [40]. We thus may combine those results to develop a magnetic exchange model which is able to describe the ground-state magnetic configurations within the Cr triangles. In particular, to get these results, we will consider collinear as well as noncollinear magnetic configurations. As already well established for CrAs [54,55], since the Cr_3As_3 -chain-based K materials may be considered as itinerant magnets, the mapping on a Heisenberg model is on the verge of applicability, so that the calculation we will present below should be considered as merely qualitative. Indeed, strictly speaking, the Heisenberg model is only justified for systems with localized moments, such as insulators or rare earth elements, but not for materials where the itinerant electrons are responsible for magnetism. Nevertheless, it may work reasonably well also for some systems belonging to this class of materials, a remarkable example being bcc Fe showing spin-spiral configurations [56]. Moreover, we point out that the Heisenberg model we put forth to capture the magnetic picture outlined in the previous section retains all the symmetries of the lattice site configurations of the systems under investigation. Therefore the calculation we will present below refers to a mapping of the DFT results into a Heisenberg model and assuming only planar configurations, as done in the previous section.

Preliminarily, we have calculated the magnetocrystalline anisotropy of 0.01 meV per magnetic atom for values of U up to 3 eV. We are thus confident that our assumption about planar configurations may produce a reasonable result. Hence we assume two independent Heisenberg coupling constants in each plane as well as two different magnetic coupling constants between the planes. We stress that, as for the first neighbors of CrAs [16,54,55], also the first neighbors of $\text{K}_2\text{Cr}_3\text{As}_3$ [39,40] are antiferromagnetically coupled. Therefore the intrachain magnetic exchanges are antiferromagnetic, the magnetic moments lying in the ab plane.

Taking into account these assumptions and considering the magnetic configurations as represented in Fig. 9, we will adopt the following Heisenberg Hamiltonian:

$$H = \sum_{\langle i,j,\mu \leq \nu \rangle} J_{i,j}^{\mu,\nu} S_i^\mu \cdot S_j^\nu. \quad (1)$$

Here, the sum is over pairs of adjacent spins in the $z = 0$ and/or $z = 0.5$ planes, and $\mu, \nu \in \{0, 1\}$. If $\mu, \nu = 0$, the spins are both in the plane located at $z = 0$; if $\mu, \nu = 1$, they both lie in the plane at $z = 0.5$; and if $\mu \neq \nu$, the two spins are in different planes. We assume mirror symmetry with respect to the y axis and a rotation of the spin at the basis of the triangles by an angle θ as shown in Fig. 9(a). In a classical picture, the total energy for a single triangle, expressed as a function of the angle θ between the spins, is given by

$$E^\mu(\theta) = S^2 [2J_a^{\mu,\mu} \cos(\theta) + J_b^{\mu,\mu} \cos(2\theta)]. \quad (2)$$

Here, the angle θ ranges from 0 to π , $J_b^{\mu,\mu}$ ($J_a^{\mu,\mu}$) is the magnetic coupling between the ions Cr_1 and Cr_3 (Cr_1 and Cr_2 or Cr_3 and Cr_2) when the ions are located at $z = 0$ ($\mu = 0$), and between the ions Cr_4 and Cr_6 (Cr_4 and Cr_5 or Cr_6 and Cr_5) when they are located at $z = 0.5$ ($\mu = 1$). Summarizing, $J_b^{0,0} = J_{1,3}^{0,0}$ and $J_b^{1,1} = J_{4,6}^{1,1}$, while $J_a^{0,0} = J_{1,2}^{0,0} = J_{3,2}^{0,0}$ and $J_a^{1,1} = J_{4,5}^{1,1} = J_{6,5}^{1,1}$.

The coupling energy between the triangles is given by

$$E^{0,1}(\theta) = S^2 [J_d^{0,1} \cos(\theta) + J_e^{0,1} \cos(2\theta)], \quad (3)$$

where $J_d^{0,1}$ and $J_e^{0,1}$ are the interplane coupling constants. Specifically, $J_d^{0,1} = J_{2,4}^{0,1} + J_{2,6}^{0,1} + J_{1,5}^{0,1} + J_{3,5}^{0,1} = 4J_{2,4}^{0,1}$ and $J_e^{0,1} = J_{1,4}^{0,1} + J_{3,6}^{0,1} = 2J_{1,4}^{0,1}$. From the available experimental data, we know that the couplings are all antiferromagnetic [39,40] and the interplane coupling constants are numerically smaller than the in-plane ones, so that $J_a^{\mu,\mu}, J_b^{\mu,\mu} > J_d^{\mu,\nu}, J_e^{\mu,\nu} > 0$. This was also verified in Appendix B.

Taking into account all the intra- and interplane interactions, we finally get the total energy $E_{\text{tot}}(\theta) = E^0(\theta) + E^1(\theta) + E^{0,1}(\theta)$ as a function of θ :

$$E_{\text{tot}}(\theta) = S^2 J_{\text{tot}} [\cos(\theta) + x \cos(2\theta)]. \quad (4)$$

Here, $J_{\text{tot}} = 2(J_a^{0,0} + J_a^{1,1}) + J_d^{0,1}$ and $x = (J_b^{0,0} + J_b^{1,1} + J_{3,1}^{0,1})/J_{\text{tot}}$. Looking at Fig. 9, we note that when $\alpha_1 = \alpha_2 = 60^\circ$, namely, when the triangles are equilateral, we have $J_a^{\mu,\mu} = J_b^{\mu,\mu}$; when $\alpha_k < 60^\circ$, $J_a^{\mu,\mu} < J_b^{\mu,\mu}$; and when $\alpha_k > 60^\circ$, $J_a^{\mu,\mu} > J_b^{\mu,\mu}$. Finally, regardless of the values of α_1 and α_2 , we have $x \leq 1$.

Studying the parametric equation (4), we find that the extreme points are given by $\theta_{\text{ext}} = 0, \pi, \arccos(-\frac{1}{4x})$. The

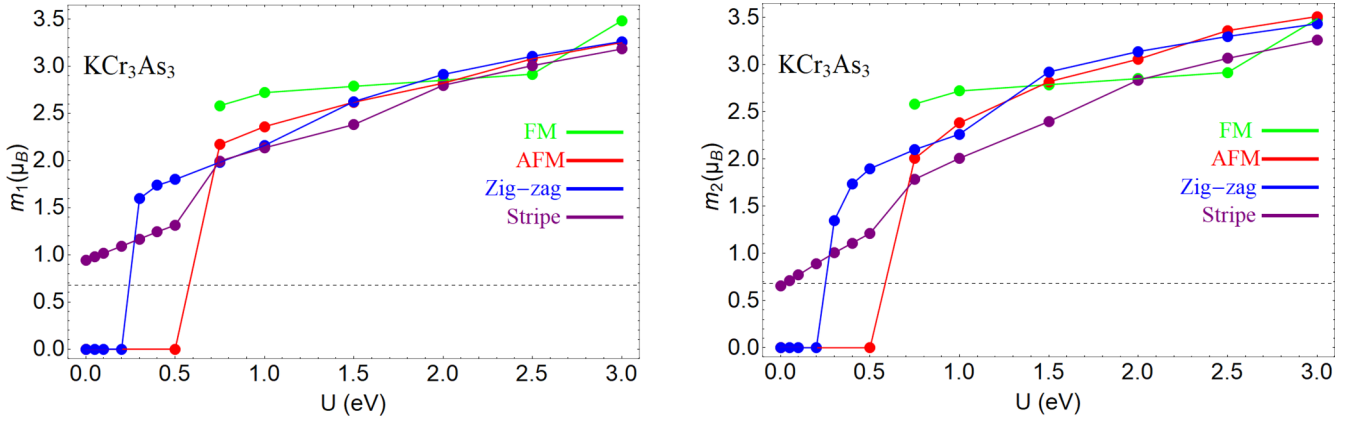


FIG. 8. Magnetic moments of the Cr atoms for the configurations shown in Fig. 2 as functions of the Coulomb interaction for the KCr_3As_3 compound. The experimental value is represented by the horizontal dashed line.

value $\theta_{\text{ext}} = 0$ gives the ferromagnetic solution [Fig. 2(a)] and corresponds to the highest-energy ground state. The second one, $\theta_{\text{ext}} = \pi$, corresponds to the collinear stripe configuration depicted in Fig. 2(c). The third one, $\theta_{\text{ext}} = \arccos(-\frac{1}{4x})$, gives a noncollinear phase corresponding to the so-called in-out solution previously investigated in the literature in the case of equilateral triangles [39,40]. We emphasize that for low values of the constant x , i.e., for $x \leq 0.25$, the lowest-energy solution corresponds to the collinear ferrimagnetic state, which we have previously called the stripe configuration, while for $x > 0.25$ the ground state becomes the noncollinear solution.

Thus this simple Heisenberg model calculation supports the DFT results presented in the previous section. Nonetheless, we stress once again that the compounds we are dealing

with are metallic, so that the outcomes presented in this section should be considered as merely qualitative.

VI. COMPARATIVE ANALYSIS OF MAGNETIC PROPERTIES OF Cr_3As_3 -CHAIN-BASED K MATERIALS

The compound KCr_3As_3 does not superconduct, and it exhibits a cluster-spin-glass behavior below $T_N = 5$ K [33]. We point out that this value is close to the superconducting critical temperature of $\text{K}_2\text{Cr}_3\text{As}_3$ [1], so that the energy scales involved in the formation of the two phases are essentially the same. At higher temperatures, it shows a Curie-Weiss behavior, indicating the presence of nonvanishing local moments [33]. Owing to the close relation with $\text{K}_2\text{Cr}_3\text{As}_3$, the presence of local-moment magnetism in KCr_3As_3 suggests that the existence of finite moments on chromium sites is detrimental to the development of a superconducting phase.

The spin-glass-like state in KCr_3As_3 seems to be associated with the geometrical frustrations in the Cr twisted tubes. Moreover, the very appearance of a superconducting phase in $\text{K}_2\text{Cr}_3\text{As}_3$, which is indeed undetected in KCr_3As_3 , may be related to the existence of unequal Cr sites [24,40,57], as recent high-pressure studies [58] suggest. In order to explore the magnetic instabilities of KCr_3As_3 and $\text{K}_2\text{Cr}_3\text{As}_3$, we extend our DFT study considering different intertube magnetic interactions [59], possibly arising in the two different space groups. For this purpose, we summarize here some of the main outcomes of the previous sections. Our DFT results predict that, for both compounds, the ground state is nonmagnetic up to a critical value U_c of the Coulomb repulsion, approximately equal to 0.25 eV for KCr_3As_3 and 0.40 eV for $\text{K}_2\text{Cr}_3\text{As}_3$. We thus have that in the interval between these two values KCr_3As_3 is magnetic while $\text{K}_2\text{Cr}_3\text{As}_3$ is nonmagnetic. We assume $U = 0.30$ eV as the value to reproduce the experimental results.

Above U_c , a collinear stripe configuration is predicted within the DWSNs, which allows us to attribute a net magnetic moment to each chain. Such a scheme is depicted in Fig. 10, where we show the macrospin \uparrow , which is associated with each chain [Fig. 10(a)]. Single interchain magnetic interactions then couple spins of neighboring chains, which are located at the sites of a triangular lattice. Without interchain

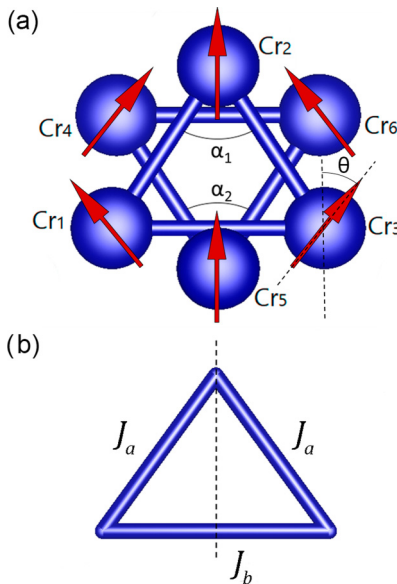


FIG. 9. (a) Magnetic arrangement of the Cr-ion magnetic moments in the $z = 0$ and $z = 0.5$ planes taken into account in the theoretical model defined by the Hamiltonian (1). (b) Exchange coupling constants: J_b is the coupling between the atoms at the basis of the triangle, while J_a is the coupling between the atom at the apex and the atom at the apex. The dashed line is the mirror axis.

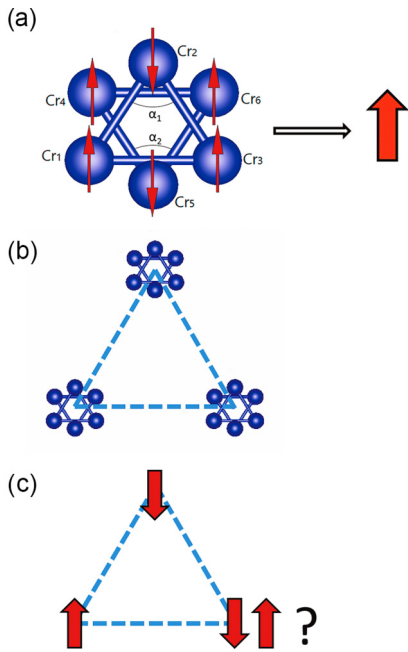


FIG. 10. (a) A net magnetic moment can be attributed to a single chain, because the ground state within the DWSNs predicted by our calculations is a collinear stripe configuration. (b) Interaction between the single chains. (c) Schematic representation of the spin-glass behavior originating from geometrical frustrations between the Cr twisted tubes.

magnetic coupling, the system can only show magnetic order in one dimension, this being difficult to achieve because of the Mermin-Wagner theorem [60,61]. With the presence of the interchain magnetic coupling, the system is not quasi-one-dimensional anymore, and a magnetic order can more easily develop. This crucial interchain magnetic coupling can be ferromagnetic or antiferromagnetic. We are going to show that in the case of ferromagnetic interchain coupling, the system is ferrimagnetic with a net magnetic moment, while in the case of antiferromagnetic interchain coupling the system is likely to exhibit a spin-glass phase.

We proceed by looking at the energy of some possible interchain magnetic configurations. In this calculation we have used the PBEsol approximation for a supercell of two chains, for which we have considered the interchain FM, the interchain AFM, and the NM phases. In the FM configuration, the chains have collinear magnetic moments $\uparrow\uparrow$, oriented in the same direction; in the AFM case they have collinear moments, which are antiparallel on the neighboring chains; and in the NM configuration, all magnetic moments are zero. Due to the estimated values of U_c , in this study we limited ourselves to analyzing the relevant cases of $U = 0, 0.3, 0.5$ eV. The results reported in Table I indicate that for $\text{K}_2\text{Cr}_3\text{As}_3$ the nonmagnetic phase is the more stable one up to $U = 0.3$ eV, whereas above this value the coupling between the chains is weakly ferromagnetic. On the other hand, in the case of KCr_3As_3 we observe that for $U \lesssim 0.25$ eV the ground state is nonmagnetic and for $U \gtrsim 0.25$ eV the ferromagnetic coupling and the antiferromagnetic coupling are almost degenerate. We used also different approximations, namely, the

TABLE I. Energy (meV) in the PBEsol approximation, measured with respect to the ground-state energy, corresponding to various interchain couplings, assuming the intrachain collinear configuration. NM, FM, and AFM indicate nonmagnetic, ferromagnetic, and antiferromagnetic interchain arrangements, respectively. Inside the chain the configuration is $\uparrow\uparrow\downarrow/\uparrow\uparrow\downarrow$.

U (eV)	$\text{K}_2\text{Cr}_3\text{As}_3$			KCr_3As_3		
	0	0.3	0.5	0	0.3	0.5
NM	0	0	19.92	0	3.75	19.33
FM	converges to NM	6.92	0	12.08	0	0
AFM	converges to NM	10.83	3.83	12.17	0.58	1.08

LDA and the meta-GGA, and we obtained similar results, confirming in KCr_3As_3 the competition between the ferromagnetic and the antiferromagnetic interactions. In Fig. 10(c) we give a schematic representation of this competition, in terms of geometrically frustrated AFM coupling between magnetic moments located at the sites of a triangular lattice. Frustration is known to be a prerequisite for the spin-glass behavior, leading to an equal probability for the spins of being aligned or antialigned and thus preventing long-range magnetic order. We propose that the magnetic coupling between the chains is antiferromagnetic for the KCr_3As_3 driving the system towards the spin-glass behavior and determining the scale of the critical temperature. Since the magnetic coupling is related to long-range hopping parameters, this coupling is expected to be relatively small, as also shown from the data in Table I. The experimental critical temperature $T_N = 5$ K is compatible with the critical temperature of other frustrated systems where the relevant magnetic coupling is not between the first-neighbor sites [62].

VII. DISCUSSION AND CONCLUSIONS

It is known that in Cr_3As_3 -chain-based K materials there is a strong interplay between spin and lattice degrees of freedom, this issue being supported by the monotonic reduction in the superconducting critical temperature with the lattice expansion produced by the substitution of the K ion with larger alkaline ions. Nevertheless, the magnetic properties of different Cr_3As_3 -chain-based K materials are rather distinct, suggesting again the important role played by the crystal structure.

In this paper we performed first-principles calculations to investigate the magnetic phases which are compatible with the orthorhombic distortion of the CrAs tubes in this family of compounds. In Fig. 11 we summarize the comparison between $\text{K}_2\text{Cr}_3\text{As}_3$ and KCr_3As_3 , by plotting the local magnetic moment at the representative Cr_1 site in the ground state, as a function of the Coulomb repulsion U . We observe that in both cases a nonvanishing magnetic moment can be attributed to the Cr sites above U_c , which slightly differs for the two compounds. Above this threshold, our DFT solution converges to a collinear stripe phase, which gives rise to a nonzero magnetization within the chain. As already pointed out in Sec. III, this calculation is performed choosing a Hund coupling $J_H = 0.15U$. To check whether the magnetic moment is

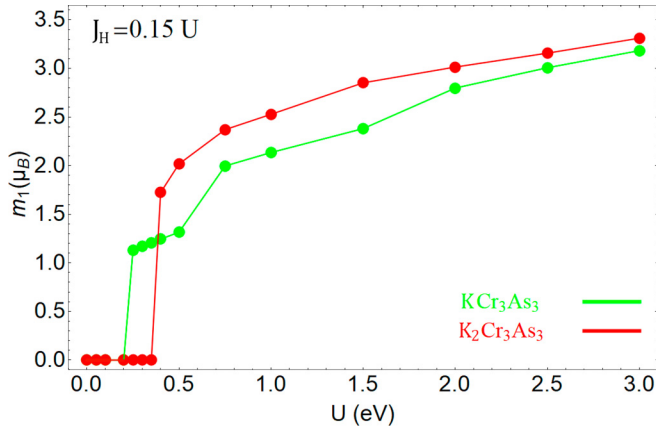


FIG. 11. Magnetic moment of the Cr_1 ion for the KCr_3As_3 and $K_2Cr_3As_3$ compounds in the ground state at $J_H = 0.15U$.

sensitive to variations in J_H , we have repeated the calculations for $J_H = 0$. We have found values of the magnetic moments only slightly greater than the ones obtained for $J_H = 0.15U$, as expected since J_H competes with the Coulomb repulsion U . However, the difference between the two cases is actually negligible, and thus the results for $J_H = 0$ are not reported here for brevity.

In the previous section we have predicted that, in the energy window $0.3 \text{ eV} \lesssim U \lesssim 0.5 \text{ eV}$ where KCr_3As_3 is in such a collinear stripe phase and the value of the magnetic moment is sufficiently close to the experimentally detected one, the ferromagnetic and antiferromagnetic couplings among the chains are close in energy. We conjecture that this result may be at the origin of a spin-glass behavior driven by the geometric frustration of the magnetic coupling among different chains, consistent with the experimental results reported by Bao *et al.* [33]. We also propose that the magnetic coupling between the chains in KCr_3As_3 determines the low critical temperature experimentally observed for the spin-glass phase [1,33].

In the same region of the parameter space, we predict $K_2Cr_3As_3$ to be nonmagnetic but on the verge of magnetism, sustaining interchain ferromagnetic spin fluctuations while the intrachain spin fluctuations are antiferromagnetic. These findings are also in agreement with previous experiments. In particular, it was reported that the imaginary part of the bare electron susceptibility of $K_2Cr_3As_3$ shows large peaks at the point Γ , suggesting the presence of large ferromagnetic spin fluctuations in the compound [39], which are robust and persist in the case of nonequilateral triangles. We note that these results suggest an analogy with the ruthenates [63–70]. Indeed, the compound Ca_2RuO_4 is magnetic with an antiferromagnetic coupling between the Ru ions [71], whereas Sr_2RuO_4 is on the verge of magnetism, exhibiting in the magnetic phase a ferromagnetic coupling among the Ru ions.

In this respect, we underline the importance of the investigation of the effects of a compressive strain applied orthogonally to the basis of the triangles in the chain of $K_2Cr_3As_3$ [72]. In a study of these effects, we have found an increase in the apical angle α which, by virtue of the above-mentioned interplay between structural properties and magnetism, enforces the stability of the magnetism [72].

Based on these arguments, it has also been demonstrated that, through a compressive strain, one can tune the superconducting $K_2Cr_3As_3$ toward a ferrimagnetic system, providing a playground to investigate the interplay between magnetism and superconductivity in this class of compounds [72].

We finally remark that our picture of $K_2Cr_3As_3$ as a moderately correlated system is consistent with angle-resolved photoemission spectroscopy (ARPES) measurements [23] showing that the overall bandwidth of the Cr $3d$ bands as well as the Fermi velocities are in agreement with the DFT results. A similar conclusion can also be inferred from a recent investigation of the band structure of this compound [27], where it has been shown that a good agreement with the results available in the literature [23,39] can be obtained for low values of the electronic correlation. We are then confident that the interesting features outlined in this paper in the moderately correlated regime are quite robust.

As a final remark, we notice that the proximity to a stripe ferrimagnetic phase within the chains may turn out to be relevant to obtain indications as to the mechanism driving the superconducting phase in $K_2Cr_3As_3$. Studies in this direction are needed.

ACKNOWLEDGMENTS

The authors acknowledge A. Galluzzi and M. Polichetti for useful discussions. G.C. acknowledges financial support from Fondazione Angelo Della Riccia. The work was supported by the Foundation for Polish Science through the International Research Agendas program cofinanced by the European Union within the Smart Growth Operational Programme. X.M. was sponsored by the National Natural Science Foundation of China (Grant No. 11864008). We acknowledge the access to the computing facilities of the Interdisciplinary Center of Modeling at the University of Warsaw, Grants No. G73-23 and No. G75-10. We acknowledge the CINECA award under the ISCRA initiatives IsC69 “MAINTOP” and IsC76 “MEPBI” grant, for the availability of high-performance computing resources and support.

APPENDIX A: ELECTRONIC PROPERTIES

In this Appendix we analyze the electronic properties of $K_2Cr_3As_3$ and KCr_3As_3 in the distorted case. As explained in Sec. III, we fix for the Coulomb repulsion the value $U = 0.3 \text{ eV}$, for which KCr_3As_3 is magnetic while $K_2Cr_3As_3$ is nonmagnetic. In Fig. 12 we report the band structure and the orbitally resolved partial densities of states (DOSs) for the d orbitals of $K_2Cr_3As_3$ near the Fermi level. We consider the partial densities of states for the d orbitals symmetric with respect to the basal plane, d_{xy} , $d_{x^2-y^2}$, and d_{z^2} , and antisymmetric with respect to the basal plane, d_{yz} and d_{xz} . We make this distinction because we know from the undistorted case [27,39] that symmetric orbitals with respect to the basal plane, d_{xy} , $d_{x^2-y^2}$, and d_{z^2} , have a greater spectral weight at the Fermi level, while the antisymmetric ones have a relevant weight a few eV from the Fermi level. In the distorted structure the atoms at $z = 0$ and $z = 0.5$ are closer than in the undistorted case, suggesting that the hybridization between the orbitals at different planes is larger, both in the symmetric and in the an-

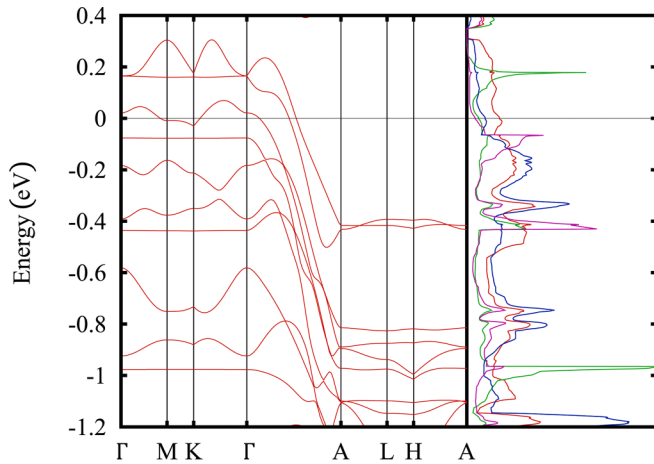


FIG. 12. Band structure of $\text{K}_2\text{Cr}_3\text{As}_3$ near the Fermi level for $U = 0.3$ eV (left), together with the corresponding orbitally resolved partial densities of states (right). Red and green lines refer to the Cr_1 atom at the basis of the triangle and denote the DOSs projected onto orbitals symmetric with respect to the basal plane, d_{xy} , $d_{x^2-y^2}$, and d_{z^2} , and onto orbitals antisymmetric with respect to the basal plane, d_{yz} and d_{xz} , respectively. Blue and purple lines refer to the Cr_2 atom at the vertex of the triangle and denote the DOSs projected onto the symmetric and antisymmetric orbitals, respectively.

tisymmetric orbital manifolds, as well as between symmetric and antisymmetric orbitals. For simplicity, we report only the results for the d orbitals because, as for the undistorted case, they encompass the largest weight at the Fermi level. We have shown in Ref. [27] that, apart from a slight increase in the energy bandwidth, corresponding to the chromium states being pushed away from the Fermi level, electronic correlations on chromium orbitals barely affect the energy spectrum. Therefore we can say that the band structure obtained for the chosen value of the Coulomb repulsion would look similar to the band structure at vanishing U . The reasonable agreement between our results and ARPES measurements [23] indicates that these materials could be considered as moderately correlated compounds that can be satisfactorily described considering small values of the Coulomb repulsion.

Since for $U = 0.3$ eV the ground state of KCr_3As_3 is magnetic, we report in Fig. 13 the band structure and the orbitally resolved partial densities of states for the d orbitals near the Fermi level, in the spin-up and in the spin-down channel, respectively. The results are in good agreement with those quoted in Ref. [43], where it is shown that the prominent three-dimensional Fermi surface in the undistorted structure is not present in the distorted case. Indeed, the band structure along the in-plane high-symmetry lines of the Brillouin zone is significantly different from the undistorted case. Actually, the bands are more flat, and the symmetry properties that allow us to connect the bands along some lines are removed by the distortion. For completeness, we noted that in our case, at $U = 0.3$ eV, the system is ferrimagnetic, which is different from Ref. [43], where the system is studied in the nonmagnetic phase.

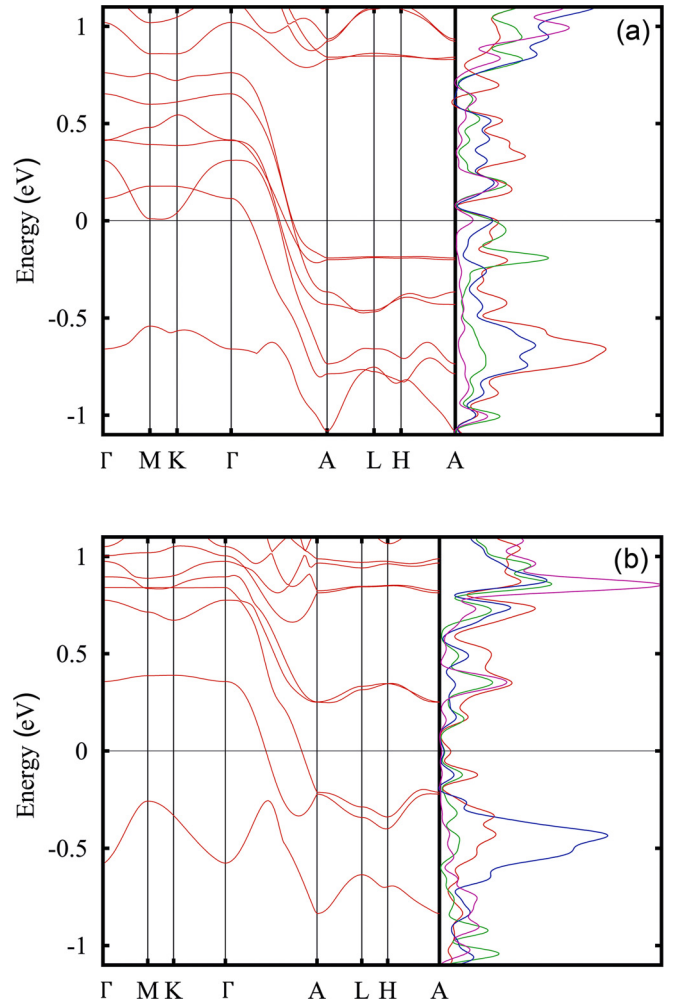


FIG. 13. (a) Band structure of KCr_3As_3 near the Fermi level for $U = 0.3$ eV (left), together with the corresponding orbitally resolved partial densities of states in the spin-up channel (right). The same colors as in Fig. 12 are used for the local DOSs. (b) The same as in (a) for the spin-down channel.

APPENDIX B: MAGNETIC EXCHANGES

In this Appendix, we map the DFT results on the Heisenberg model providing an estimation of the exchange couplings and explaining the limitations of the method for this class of materials. The mapping of the DFT results on the Heisenberg model relies on the calculation of the energy of several magnetic configurations. The reliability of this method largely depends on the values of the magnetic moments that should be constant in these different configurations. As shown in Figs. 5 and 8, while the magnetic moments are approximately constant in the various magnetic phases for $U \gtrsim 1.5$ eV, they strongly differ for $U < 1.5$ eV. However, our results show that it is still possible to perform the mapping to the Heisenberg model for 0.75 eV $\lesssim U < 1.5$ eV in the case of $\text{K}_2\text{Cr}_3\text{As}_3$, and for 1.2 eV $\lesssim U < 1.5$ eV in the case of KCr_3As_3 , though we are on the verge of the applicability of the mapping for these materials. Since we know that the magnetic coupling should go to zero for U approximately lower than 0.4 eV [73], in the case of $\text{K}_2\text{Cr}_3\text{As}_3$ we may roughly

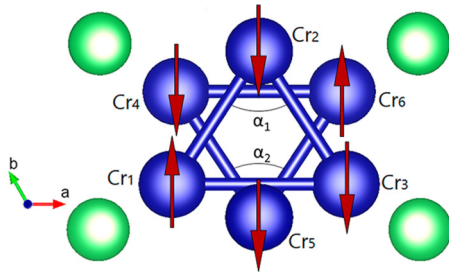


FIG. 14. Arrangements of the Cr spin of the additional magnetic configuration investigated to obtain the magnetic exchanges. The Cr atoms at the basis of the triangles have opposite moment directions.

extrapolate the value of J from $U = 0.75$ eV to $U = 0.30$ eV [as shown by the dashed lines in Fig. 15(a)]. Similarly, in the case of KCr_3As_3 we are able to reliably calculate the magnetic couplings up to $U = 1.2$ eV, and, as in the previous case, we extrapolate an estimation of the exchange couplings considering that they should go to zero for U lower than 0.3 eV [dashed lines in Fig. 15(b)]. We note that in order to assess the first-neighbor magnetic coupling, we assume that the two interlayer ones are equal, namely, $J_{2,4}^{0,1} = J_{1,4}^{0,1}$ (the same notation as in Sec. V is here adopted), and we have calculated the energy also considering the magnetic configuration plotted in Fig. 14. We see that in this additional configuration, the spins of the Cr atoms at the basis of the triangles have opposite directions. For completeness, we point out that we have excluded from our evaluation the ferromagnetic phase configuration since it can be obtained from a suitable linear combination of the other phases. We indicate with J_a the magnetic coupling between the Cr at the apex and the Cr at the basis of the isosceles triangles, while J_b is the magnetic coupling between the two Cr atoms of the basis. J_c is the interplane coupling constant; $J_c = J_{2,4}^{0,1} = J_{1,4}^{0,1}$ using the notation of the Sec. V. The results we obtain for the magnetic exchanges as U is varied are reported in Fig. 15(a) for $\text{K}_2\text{Cr}_3\text{As}_3$ and in Fig. 15(b) for KCr_3As_3 . From an inspection of these figures, we infer that the magnetic exchanges for KCr_3As_3 are on average larger than the magnetic exchanges for $\text{K}_2\text{Cr}_3\text{As}_3$. Also, all the first-neighbor magnetic exchanges are antiferromagnetic, for every value of U , including the case $U = 2$ eV previously reported for the undistorted case [40]. In both cases, the in-plane magnetic coupling J_a is larger than J_b , stabilizing the collinear magnetic configuration, as reported in the main text. Furthermore, the interlayer magnetic

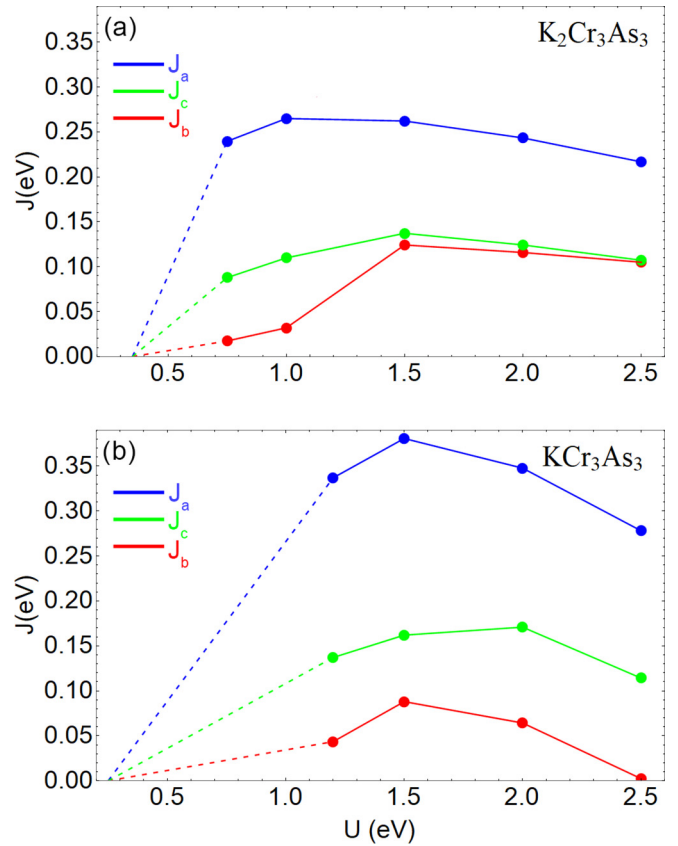


FIG. 15. (a) Magnetic exchanges for the $\text{K}_2\text{Cr}_3\text{As}_3$ as a function of the Coulomb repulsion U . J_a , J_b , and J_c are three magnetic exchanges described in the text. The dashed lines indicate the extrapolation of the couplings in the region where mapping is not possible. (b) The same as in (a) for KCr_3As_3 .

coupling J_c is larger than the previously calculated magnetic couplings [40], and we attribute this difference to the effect of the distortions that reduces the interlayer Cr-Cr bonds and, consequentially, increases the coupling between the magnetic moments.

Finally, as far as the estimation of the critical temperature is concerned, we note that the systems investigated here are quasi-one-dimensional with frustrated magnetism. Accordingly, a mean-field approach fails to provide a correct estimation of T_c . This would rather require the inclusion in the calculation of the interchain exchange interactions, but this is beyond the scope of this paper.

[1] J.-K. Bao, J.-Y. Liu, C.-W. Ma, Z.-H. Meng, Z.-T. Tang, Y.-L. Sun, H.-F. Zhai, H. Jiang, H. Bai, C.-M. Feng, Z.-A. Xu, and G.-H. Cao, *Phys. Rev. X* **5**, 011013 (2015).
 [2] Q.-G. Mu, B.-B. Ruan, B.-J. Pan, T. Liu, J. Yu, K. Zhao, G.-F. Chen, and Z.-A. Ren, *Phys. Rev. Materials* **2**, 034803 (2018).
 [3] Z.-T. Tang, J.-K. Bao, Y. Liu, Y.-L. Sun, A. Ablimit, H.-F. Zhai, H. Jiang, C.-M. Feng, Z.-A. Xu, and G.-H. Cao, *Phys. Rev. B* **91**, 020506(R) (2015).

[4] Z.-T. Tang, J.-K. Bao, Z. Wang, H. Bai, H. Jiang, Y. Liu, H.-F. Zhai, C.-M. Feng, Z.-A. Xu, and G.-H. Cao, *Sci. China Mater.* **58**, 16 (2015).
 [5] G. Goll, *Unconventional Superconductors* (Springer, Berlin, 2006).
 [6] M. N. Norman, *Science* **332**, 196 (2011).
 [7] H. Z. Zhi, T. Imai, F. L. Ning, J.-K. Bao, and G.-H. Cao, *Phys. Rev. Lett.* **114**, 147004 (2015).

- [8] D. T. Adroja, A. Bhattacharyya, M. Telling, Y. Feng, M. Smidman, B. Pan, J. Zhao, A. D. Hillier, F. L. Pratt, and A. M. Strydom, *Phys. Rev. B* **92**, 134505 (2015).
- [9] G. M. Pang, M. Smidman, W. B. Jiang, J. K. Bao, Z. F. Weng, Y. F. Wang, L. Jiao, J. L. Zhang, G. H. Cao, and H. Q. Yuan, *Phys. Rev. B* **91**, 220502(R) (2015).
- [10] C. Noce, *EPL (Europhys. Lett.)* **130**, 67001 (2020).
- [11] H.-T. Zhong, X.-Y. Feng, H. Chen, and J.-H. Dai, *Phys. Rev. Lett.* **115**, 227001 (2015).
- [12] R. Y. Chen and N. L. Wang, *Rep. Prog. Phys.* **82**, 012503 (2019).
- [13] W. Wu, X. Zhang, Z. Yin, P. Zheng, N. Wang, and J. Luo, *Sci. China: Phys. Mech. Astron.* **53**, 1207 (2010).
- [14] W. Wu, L. Cheng, K. Matsubayashi, P. Kong, F. Lin, C. Jin, N. Wang, Y. Uwatoko, and J. Luo, *Nat. Commun.* **5**, 5508 (2014).
- [15] H. Kotegawa, S. Nakahara, H. Tou, and H. Sugawara, *J. Phys. Soc. Jpn.* **83**, 093702 (2014).
- [16] C. Autieri and C. Noce, *Philos. Mag.* **97**, 3276 (2017).
- [17] C. Autieri, G. Cuono, F. Forte, and C. Noce, *J. Phys.: Condens. Matter* **29**, 224004 (2017).
- [18] C. Autieri, G. Cuono, F. Forte, and C. Noce, *J. Phys.: Conf. Ser.* **969**, 012106 (2018).
- [19] G. Cuono, C. Autieri, G. Guarnaccia, A. Avella, M. Cuoco, F. Forte, and C. Noce, *Eur. Phys. J.: Spec. Top.* **228**, 631 (2019).
- [20] G. Cuono, F. Forte, M. Cuoco, R. Islam, J. Luo, C. Noce, and C. Autieri, *Phys. Rev. Materials* **3**, 095004 (2019).
- [21] A. Nigro, P. Marra, C. Autieri, W. Wu, J. G. Cheng, J. Luo, and C. Noce, *EPL (Europhys. Lett.)* **125**, 57002 (2019).
- [22] T. Kong, S. L. Bud'ko, and P. C. Canfield, *Phys. Rev. B* **91**, 020507(R) (2015).
- [23] M. D. Watson, Y. Feng, C. W. Nicholson, C. Monney, J. M. Riley, H. Iwasawa, K. Refson, V. Sacksteder, D. T. Adroja, J. Zhao, and M. Hoesch, *Phys. Rev. Lett.* **118**, 097002 (2017).
- [24] G.-H. Cao, J.-K. Bao, Z.-T. Tang, Y. Liu, and H. Jiang, *Philos. Mag.* **97**, 8 (2017).
- [25] G.-H. Cao and Z.-W. Zhu, *Chin. Phys. B* **27**, 107401 (2018).
- [26] G. Cuono, C. Autieri, F. Forte, G. Busiello, M. T. Mercaldo, A. Romano, C. Noce, and A. Avella, *AIP Adv.* **8**, 101312 (2018).
- [27] G. Cuono, C. Autieri, F. Forte, M. T. Mercaldo, A. Romano, A. Avella, and C. Noce, *New J. Phys.* **21**, 063027 (2019).
- [28] S. Reja and S. Nishimoto, *Sci. Rep.* **9**, 2691 (2019).
- [29] W. Wang, B. Wang, Z. Gao, G. Tang, W. Lei, X. Zheng, H. Li, X. Ming, and C. Autieri, *Phys. Rev. B* **102**, 155115 (2020).
- [30] B. Sipoš, A. F. Kusmartseva, A. Akrap, H. Berger, L. Forró, and E. Tutiš, *Nat. Mater.* **7**, 960 (2008).
- [31] E. Martino, A. Pisoni, L. Ćirić, A. Arakcheeva, H. Berger, A. Akrap, C. Putzke, P. J. W. Moll, I. Batistić, E. Tutiš, L. Forró, and K. Semeniuk, *npj 2D Mater. Appl.* **4**, 7 (2020).
- [32] D. Wickramaratne, S. Khmelevskiy, D. F. Agterberg, and I. I. Mazin, *Phys. Rev. X* **10**, 041003 (2020).
- [33] J.-K. Bao, L. Li, Z.-T. Tang, Y. Liu, Y.-K. Li, H. Bai, C.-M. Feng, Z.-A. Xu, and G.-H. Cao, *Phys. Rev. B* **91**, 180404(R) (2015).
- [34] Q. G. Mu, B. B. Ruan, B. J. Pan, T. Liu, J. Yu, K. Zhao, G. F. Chen, and Z. A. Ren, *Phys. Rev. B* **96**, 140504(R) (2017).
- [35] T. Liu, Q. G. Mu, B. J. Pan, J. Yu, B. B. Ruan, K. Zhao, G. F. Chen, and Z. A. Ren, *EPL (Europhys. Lett.)* **120**, 27006 (2018).
- [36] K. M. Taddei, L. D. Sanjeewa, B.-H. Lei, Y. Fu, Q. Zheng, D. J. Singh, A. S. Sefat, and C. de la Cruz, *Phys. Rev. B* **100**, 220503(R) (2019).
- [37] S.-Q. Wu, C. Cao, and G.-H. Cao, *Phys. Rev. B* **100**, 155108 (2019).
- [38] J.-J. Xiang, Y.-T. Shao, Y.-W. Cui, L.-P. Nie, S.-Q. Wu, B.-Z. Li, Z. Ren, T. Wu, and G.-H. Cao, *Phys. Rev. Materials* **4**, 124802 (2020).
- [39] H. Jiang, G. Cao, and C. Cao, *Sci. Rep.* **5**, 16054 (2015).
- [40] X.-X. Wu, C.-C. Le, J. Yuan, H. Fan, and J.-P. Hu, *Chin. Phys. Lett.* **32**, 057401 (2015).
- [41] J. Luo, J. Yang, R. Zhou, Q. G. Mu, T. Liu, Z.-A. Ren, C. J. Yi, Y. G. Shi, and G.-Q. Zheng, *Phys. Rev. Lett.* **123**, 047001 (2019).
- [42] K. M. Taddei, G. Xing, J. Sun, Y. Fu, Y. Li, Q. Zheng, A. S. Sefat, D. J. Singh, and C. de la Cruz, *Phys. Rev. Lett.* **121**, 187002 (2018).
- [43] G. Xing, L. Shang, Y. Fu, W. Ren, X. Fan, W. Zheng, and D. J. Singh, *Phys. Rev. B* **99**, 174508 (2019).
- [44] C. Xu, N. Wu, G.-X. Zhi, B.-H. Lei, X. Duan, F. Ning, C. Cao, and Q. Chen, *npj Comput. Mater.* **6**, 30 (2020).
- [45] G. Kresse and J. Hafner, *Phys. Rev. B* **47**, 558 (1993).
- [46] G. Kresse and J. Furthmüller, *Comput. Mater. Sci.* **6**, 15 (1996).
- [47] G. Kresse and J. Furthmüller, *Phys. Rev. B* **54**, 11169 (1996).
- [48] G. Kresse and D. Joubert, *Phys. Rev. B* **59**, 1758 (1999).
- [49] J. P. Perdew, A. Ruzsinszky, G. I. Csonka, O. A. Vydrov, G. E. Scuseria, L. A. Constantin, X. Zhou, and K. Burke, *Phys. Rev. Lett.* **100**, 136406 (2008).
- [50] A. I. Liechtenstein, V. I. Anisimov, and J. Zaanen, *Phys. Rev. B* **52**, R5467(R) (1995).
- [51] A. Georges, L. De' Medici, and J. Mravlje, *Annu. Rev. Condens. Matter Phys.* **4**, 137 (2013).
- [52] L. Vaugier, H. Jiang, and S. Biermann, *Phys. Rev. B* **86**, 165105 (2012).
- [53] J. Sun, A. Ruzsinszky, and J. P. Perdew, *Phys. Rev. Lett.* **115**, 036402 (2015).
- [54] M. Matsuda, F. K. Lin, R. Yu, J.-G. Cheng, W. Wu, J. P. Sun, J. H. Zhang, P. J. Sun, K. Matsubayashi, T. Miyake, T. Kato, J.-Q. Yan, M. B. Stone, Q. Si, J. L. Luo, and Y. Uwatoko, *Phys. Rev. X* **8**, 031017 (2018).
- [55] K. Sen, Y. Yao, R. Heid, A. Omoumi, F. Hardy, K. Willa, M. Merz, A. A. Haghighirad, and M. Le Tacon, *Phys. Rev. B* **100**, 104301 (2019).
- [56] R. Singer, F. Dietermann, and M. Fähnle, *Phys. Rev. Lett.* **107**, 017204 (2011).
- [57] X. X. Wu, F. Yang, C. C. Le, H. Fan, and J. P. Hu, *Phys. Rev. B* **92**, 104511 (2015).
- [58] Z. Wang, W. Yi, Q. Wu, V. A. Sidorov, J. Bao, Z. Tang, J. Guo, Y. Zhou, S. Zhang, H. Li, Y. Shi, X. Wu, L. Zhang, K. Yang, A. Li, G. Cao, J. Hu, L. Sun, and Z. Zhao, *Sci. Rep.* **6**, 37878 (2016).
- [59] G. Cuono, C. Autieri, and M. M. Wysokiński, *arXiv:2104.04245*.
- [60] A. Gelfert and W. Nolting, *J. Phys: Condens. Matter* **13**, 505 (2001).
- [61] C. Noce, *Phys. Rep.* **431**, 173 (2006).
- [62] S. A. Ivanov, A. A. Bush, A. I. Stash, K. E. Kamentsev, V. Y. Shkuratov, Y. O. Kvashnin, C. Autieri, I. Di Marco, B. Sanyal, O. Eriksson, P. Nordblad, and R. Mathieu, *Inorg. Chem.* **55**, 2791 (2016).
- [63] A. P. Mackenzie and Y. Maeno, *Rev. Mod. Phys.* **75**, 657 (2003).
- [64] M. Cuoco, F. Forte, and C. Noce, *Phys. Rev. B* **73**, 094428 (2006).

- [65] M. Cuoco, F. Forte, and C. Noce, [Phys. Rev. B **74**, 195124 \(2006\)](#).
- [66] F. Forte, M. Cuoco, and C. Noce, [Phys. Rev. B **82**, 155104 \(2010\)](#).
- [67] C. Autieri, M. Cuoco, and C. Noce, [Phys. Rev. B **85**, 075126 \(2012\)](#).
- [68] M. Malvestuto, V. Capogrosso, E. Carleschi, L. Galli, E. Gorelov, E. Pavarini, R. Fittipaldi, F. Forte, M. Cuoco, A. Vecchione, and F. Parmigiani, [Phys. Rev. B **88**, 195143 \(2013\)](#).
- [69] C. Autieri, M. Cuoco, and C. Noce, [Phys. Rev. B **89**, 075102 \(2014\)](#).
- [70] V. Granata, L. Capogna, F. Forte, M.-B. Lepetit, R. Fittipaldi, A. Stunault, M. Cuoco, and A. Vecchione, [Phys. Rev. B **93**, 115128 \(2016\)](#).
- [71] D. G. Porter, V. Granata, F. Forte, S. Di Matteo, M. Cuoco, R. Fittipaldi, A. Vecchione, and A. Bombardi, [Phys. Rev. B **98**, 125142 \(2018\)](#).
- [72] G. Cuono, F. Forte, A. Romano, X. Ming, J. Luo, C. Autieri, and C. Noce, [Phys. Rev. Materials **5**, 064402 \(2021\)](#).
- [73] A. Galluzzi, G. Cuono, A. Romano, J. Luo, C. Autieri, C. Noce, and M. Polichetti (unpublished).